Society of Medical Education & Research

2025, Volume 5, Issue 1, Page No: 99-116
ISSN: 3108-4834

Archive of International Journal of Cancer and Allied Science

FTO/YTHDF2 Axis Mediates AKT Inhibition-Induced Ferroptosis by Enhancing GPX4 m⁶A Methylation and Degradation in Colorectal Cancer

Elzbieta Anna Kowalska[1]*, Magdalena Joanna Zielinska[1]

[1]Department of Oncology, Medical University of Gdansk, Gdansk, Poland.

***E-mail** ✉ e.kowalska.mug@outlook.com

Abstract

Ferroptosis represents a recently identified form of programmed cell death that depends on iron and is triggered by lipid peroxidation. Nevertheless, its precise mechanisms and therapeutic relevance in cancer, particularly at the level of post-transcriptional regulation, remain largely unclear. In this study, we demonstrated that AKT inhibition markedly triggered GPX4-dependent ferroptosis and effectively restrained colorectal cancer progression both in vitro and in vivo. This process was accompanied by suppression of the demethylase FTO, leading to elevated m6A modification of GPX4 mRNA, which was then recognized by YTHDF2 and subsequently degraded. Bioinformatic prediction identified three putative methylation sites (193/647/766), among which site 193 was confirmed as the functional locus, being demethylated by FTO and recognized by YTHDF2. Meanwhile, inhibition of AKT promoted reactive oxygen species (ROS) accumulation, which exerted negative feedback regulation on GPX4 expression. Furthermore, MK2206 treatment initiated a protective autophagy response, whereas autophagy blockade further intensified ferroptosis and significantly potentiated the antitumor efficacy of MK2206. Overall, AKT suppression activated ferroptosis via the FTO/YTHDF2/GPX4 axis to inhibit colon cancer development, highlighting FTO and GPX4 as promising biomarkers and therapeutic targets in colorectal cancer management.

Keywords: Colorectal cancer, Ferroptosis, m6A, Cancer development

Introduction

Colorectal cancer (CRC) ranks as the third most prevalent malignancy worldwide in terms of both incidence and mortality [1]. Each year, more than 1.8 million new CRC cases are diagnosed globally, with approximately 850,000 deaths attributed to this disease [2]. Surgical resection remains the primary treatment approach; however, a substantial proportion of patients still experience postoperative recurrence after surgery [3]. Therefore, there is an urgent need to identify novel therapeutic strategies to limit tumor progression and improve clinical outcomes in CRC patients.

The PI3K–AKT signaling cascade plays a central role in multiple biological processes, including cellular growth, proliferation, and metabolism [4]. AKT activation enhances tumor cell proliferation across various cancer types and contributes to resistance against anticancer therapies and cell death. In contrast, AKT inhibition diminishes cell viability and is considered a promising therapeutic strategy to augment antitumor efficacy, particularly in drug-resistant settings [5]. Current evidence links AKT closely to several forms of regulated cell death, including pyroptosis, apoptosis, autophagy, parthanatos, and ferroptosis [6]. However, the detailed mechanisms by which AKT modulates ferroptosis remain to be fully elucidated.

Ferroptosis is an iron-dependent form of regulated cell death driven by lipid peroxidation and was identified only recently [7]. Its morphological features, molecular

Access this article online https://smerpub.com/

Received: 28 February 2025; **Accepted:** 03 June 2025

How to cite this article: Kowalska EA, Zielinska MJ. FTO/YTHDF2 Axis Mediates AKT Inhibition-Induced Ferroptosis by Enhancing GPX4 m⁶A Methylation and Degradation in Colorectal Cancer. Arch Int J Cancer Allied Sci. 2025;5(1):99-116. https://doi.org/10.51847/98RN15K5Zx

pathways, and execution mechanisms are fundamentally distinct from other programmed cell death types [8], such as apoptosis, necroptosis, pyroptosis, and cuprotosis [9-11]. Hallmarks of ferroptosis include iron-dependent lipid oxidative damage, degradation of glutathione peroxidase 4 (GPX4), and increased mitochondrial membrane density [12]. Emerging studies indicate that ferroptosis regulation is closely associated with autophagy [13, 14], although the exact relationship remains insufficiently defined.

N6-methyladenosine (m6A) modification is the most prevalent post-transcriptional modification on mRNA [15] and is dynamically regulated by "writers" (methyltransferases), "erasers" (demethylases), and "readers" (m6A-binding proteins) [16]. Writers, including METTL3, METTL14, METTL16, WTAP, and KIAA1429, catalyze m6A deposition [17, 18]. Erasers such as FTO and ALKBH5 remove m6A marks, enabling reversible regulation [19]. Readers, including members of the YTH domain family and IGF2BP family [20, 21], such as YTHDF1-3 and YTHDC1-2, interpret m6A signals to modulate mRNA fate.

In our earlier work, we showed that ERK inhibition could trigger protective autophagy in colorectal cancer cells [22]. However, whether a similar protective autophagy mechanism operates during ferroptosis has not been fully clarified. Moreover, the involvement of post-transcriptional mechanisms, particularly m6A RNA modification, in ferroptosis remains largely unexplored. In the present study, we identified a previously unrecognized post-transcriptional regulatory pathway in which AKT inhibition reduced FTO expression, thereby decreasing GPX4 levels in a YTHDF2-dependent manner, and confirmed site 193 as a bona fide methylation site on GPX4 mRNA. Additionally, we demonstrated the existence of protective autophagy during ferroptosis.

Materials and Methods

Cell culture

HCT-116 and SW480 cell lines were obtained from the American Type Culture Collection. HCT-116 cells were maintained in DMEM (Gibco, Carlsbad, USA), while SW480 cells were cultured in L-15 medium (KeyGEN BioTECH, China), both supplemented with 10% fetal bovine serum (FBS; Gibco, USA) and 1% penicillin–streptomycin (NCM Biotech, China). Cells were incubated at 37 °C in an atmosphere containing 5% CO_2. All cell lines were routinely tested and confirmed to be free of mycoplasma contamination.

Reagents and antibodies

Chloroquine (CQ) was purchased from Solarbio (Beijing, China). RSL3, Fer-1, FB23-2, DC661, Z-VAD, and NAC were obtained from Selleck Chemicals (Houston, TX, USA). MK2206 was acquired from Topscience (Shanghai, China). Primary antibodies against m6A, LC3, Ki67, AKT, p-AKT, FTO, YTHDF1, YTHDF2, YTHDF3, FN1, and β-actin were sourced from Proteintech (Wuhan, China), whereas antibodies against GPX4, SIRT6, and p-SIRT6 were obtained from Abcam (Cambridge, UK).

Western blotting

Total protein was extracted using lysis buffer for Western blotting and immunoprecipitation (Beyotime, China), followed by separation on SDS–PAGE gels. Proteins were transferred onto PVDF membranes (Millipore, USA), which were blocked with 5% BSA for 1 h at 25 °C. Membranes were incubated with the appropriate primary antibodies at 4 °C overnight, then with secondary antibodies for 1 h at 25 °C. Protein signals were visualized using a chemiluminescence imaging system, and relative expression levels were quantified. All western blot data are provided in the Supplementary Material.

RT–qPCR

Total RNA was isolated using TRIzol reagent and reverse-transcribed into cDNA with the HiScript Q RT SuperMix for qPCR Kit (Vazyme, Nanjing, China). Quantitative PCR was performed using the ChamQ Universal SYBR qPCR Master Mix (Vazyme, Nanjing, China), and relative mRNA levels were calculated using the 2^−ΔΔCt method, normalized to β-actin.

MeRIP–qPCR

An MeRIP Kit (Epigentek, USA) was employed to enrich mRNA fragments containing m6A modifications from total RNA. GPX4 m6A methylation levels were then quantified by qPCR using site-specific primers.

Immunohistochemistry staining

Tumor specimens were fixed in 4% paraformaldehyde for 24 h and subsequently dehydrated through graded alcohols and xylene before paraffin embedding. Sections (5 μm) were prepared, and antigen retrieval was blocked

using 1% hydrogen peroxide. Slides were incubated with primary antibodies at 4 °C overnight, followed by secondary antibody incubation at room temperature for 30 min. After DAB chromogenic development, tissues were dehydrated and mounted with neutral resin. Images were evaluated under a light microscope by three experienced investigators [23].

m6A dot blot assay

Total RNA extracted from cells or tissues was denatured at 70 °C for 10 min, rapidly chilled on ice for at least 2 min, and aliquoted into 200 ng, 400 ng, and 800 ng samples. Equal volumes were spotted onto nylon membranes (Beyotime, Shanghai, China) and baked at 80 °C for 2 h to immobilize RNA. Membrane blocking and antibody incubation followed the same protocol as western blotting, and signal detection was performed similarly.

Cell viability assays and colony formation

CRC cells (5×10^3 per well) were seeded into 96-well plates. After 24 h, the culture medium was replaced with treatment-specific media, and absorbance at 450 nm was measured at the indicated time points using a microplate reader. Cell viability was assessed with the Cell Counting Kit-8 (CCK-8; APExBIO, Houston, USA). For colony formation assays, 1×10^3 cells were plated in 6-well plates and cultured for 2 weeks with appropriate treatments, followed by fixation with paraformaldehyde, crystal violet staining, and imaging.

ROS detection and measurement

Intracellular ROS levels were determined using a ROS Assay Kit (Beyotime, Shanghai, China). After 24 h of treatment, cells were incubated with 10 μM/mL DCFH-DA for 30 min, washed three times with PBS, and imaged under a fluorescence microscope. Quantification of ROS-positive cells was performed using ImageJ software.

Cell transfection and RNA interference

shRNA plasmids targeting AKT were obtained from Hansheng Technology, and all siRNAs were purchased from GenePharma (Shanghai, China). Stable shAKT cell lines were generated using 293T cells. Plasmids were transfected into 293T cells with Lipofectamine 2000 (Invitrogen, USA), and viral supernatants were collected and used to infect HCT-116 cells at 24 h, 48 h, and 72 h. siRNAs were transfected into target cells using Lipofectamine 2000. After 24 h, the medium was replaced, and cells were incubated for an additional 24 h prior to further treatments.

EDU assay

Cell proliferation was assessed using an EdU incorporation assay. CRC cells (5×10^4 per well) were seeded in 24-well plates and treated for 24 h, followed by incubation with 10 μM EdU for 2 h at 37 °C. Cells were fixed with 4% formaldehyde for 15 min, washed with PBS, permeabilized with 0.1% Triton X-100 for 10 min, and stained with EdU solution and Hoechst for nuclear labeling. Images were captured using a fluorescence microscope.

Animal models

Female BALB/c nude mice (6–8 weeks old) were randomly assigned to four groups (Control, MK2206, CQ, MK2206 + CQ; n = 4 per group). CRC cells (1×10^6) suspended in 100 μL PBS were injected subcutaneously into the left axilla under sterile conditions. When tumors reached approximately 50 mm^3, mice were treated with MK2206 (90 mg/kg, oral gavage) [24] and/or CQ (25 mg/kg, intraperitoneal injection) [22]. Control mice received equal volumes of 0.9% NaCl and sodium carboxymethyl cellulose solution by gavage. Tumor size and body weight were recorded every 2 days, and mice were euthanized after 14 days of treatment. Tumor volume was calculated using the formula:

$$1/2 \times (\text{length} \times \text{width}^2). \quad (1)$$

Statistical analysis

All experiments were performed at least three times independently. Data were analyzed using GraphPad Prism 7.0 and are presented as mean ± SEM. Statistical significance was determined using Student's paired *t*-test.

Results and Discussion

AKT inhibition suppressed colorectal cancer cell proliferation

To assess the critical involvement of the AKT pathway in CRC initiation and progression, the AKT inhibitor MK2206 was applied, and the appropriate treatment dose and duration were first determined. HCT-116 and SW480 cells were exposed to increasing concentrations of MK2206 (1, 2, 5, and 10 μM), and cell viability was measured using the CCK-8 assay at 0, 12, 24, 36, and

48 h. A progressive decline in proliferative capacity was observed in CRC cells with increasing drug concentration and prolonged exposure **(Figures 1and 1b).** Consistently, colony formation ability was markedly reduced following 3 days of treatment with 10 μM MK2206 **(Figure 1c).** EDU incorporation assays further confirmed these inhibitory effects on cell proliferation **(Figures 1d–1f).** Subsequently, phosphorylated AKT (P-AKT) levels were examined and found to be substantially decreased after MK2206 treatment **(Figures 1g–1i)**. As a direct downstream effector of AKT, the phosphorylation status of 4EBP1 (P-4EBP1) was analyzed alongside P-AKT following exposure to MK2206 (1, 2, 5, and 10 μM). The data indicated that lower concentrations (1 or 2 μM) were sufficient to inactivate 4EBP1, whereas higher concentrations (5 or 10 μM) were required for robust AKT inhibition. Collectively, these findings demonstrated that AKT targeting effectively restrained CRC cell growth, prompting further exploration of the underlying mechanisms.

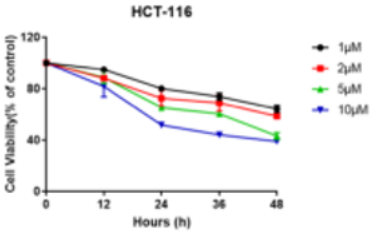

a)

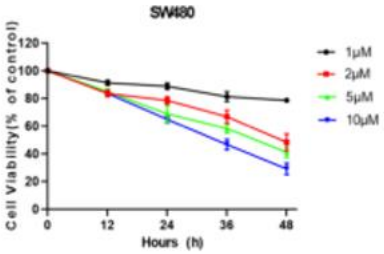

b)

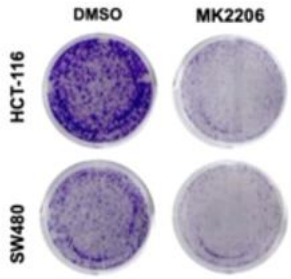

c)

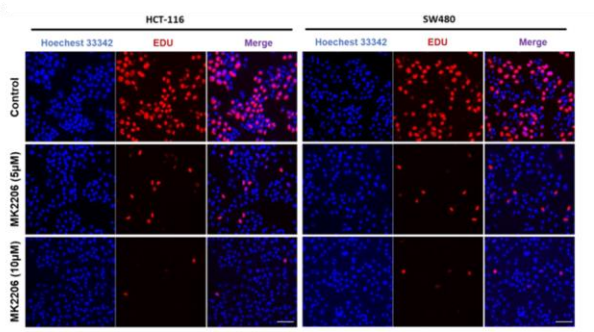

d)

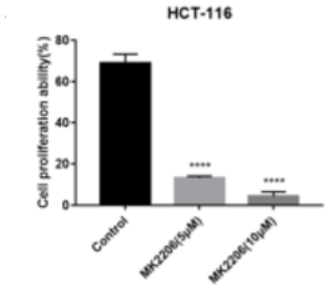

e)

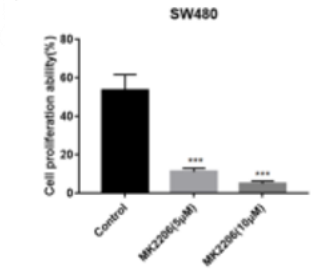

f)

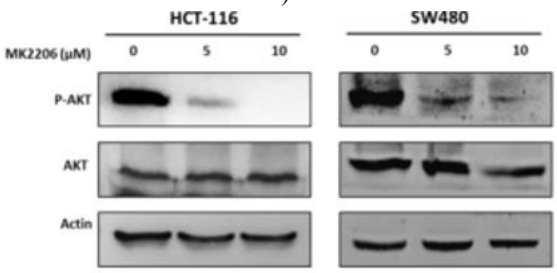

g)

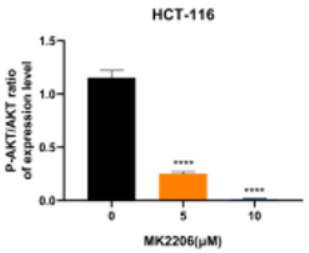

h)

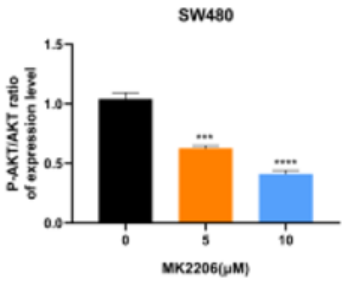

i)

Figure 1. MK2206 suppressed proliferation in CRC cells.

a, b) HCT-116 and SW480 cells were treated with various concentrations of MK2206 for 12, 24, 36, and 48 h, followed by assessment of cell viability using the CCK-8 assay.

c) Colony formation assays of HCT-116 and SW480 cells treated with 10 μM MK2206 for 2 weeks.

d–f) Cell proliferation was evaluated by EDU staining after exposure to 5 μM and 10 μM MK2206 [scale bar, 100 μm].

g–i) HCT-116 and SW480 cells were treated with 0, 5, and 10 μM MK2206 for 24 h, after which P-AKT, total AKT, and β-Actin protein levels were examined by western blotting.

AKT targeting triggered ferroptosis

Following treatment with 5 and 10 μM MK2206, GPX4 protein expression was examined and found to be markedly reduced **(Figures 2a–2c).** Similarly, AKT knockdown produced comparable decreases in GPX4 levels **(Figures 2d and 2e).** Because GPX4 downregulation is accompanied by enhanced reactive oxygen species (ROS) accumulation, a hallmark of ferroptosis, intracellular ROS levels were measured, with RSL3 (a ferroptosis inducer) included as a positive control. ROS production was significantly elevated after MK2206 exposure, comparable to that induced by RSL3 **(Figures 2f–2h),** further supporting ferroptosis activation. Notably, this increase in ROS was strongly attenuated by Fer-1 (a ferroptosis inhibitor) or NAC (a ROS scavenger), consistent with expectations. Altogether, AKT inhibition reduced GPX4 protein abundance and enhanced ROS accumulation, indicating that suppression of AKT promoted ferroptosis through GPX4 downregulation.

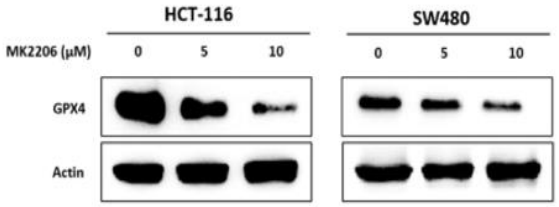

a)

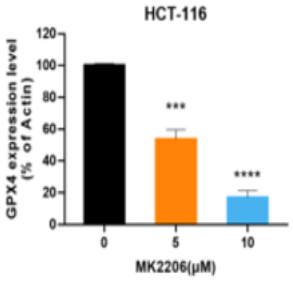

b)

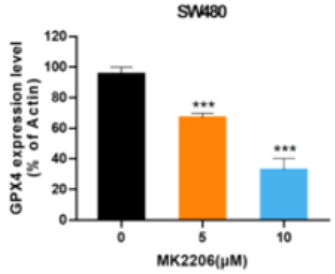

c)

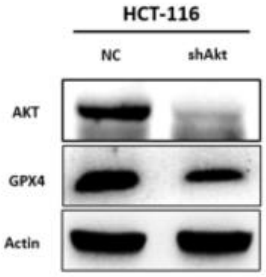

d)

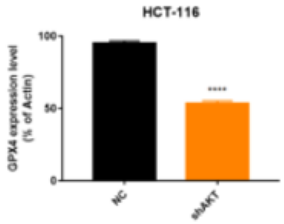

e)

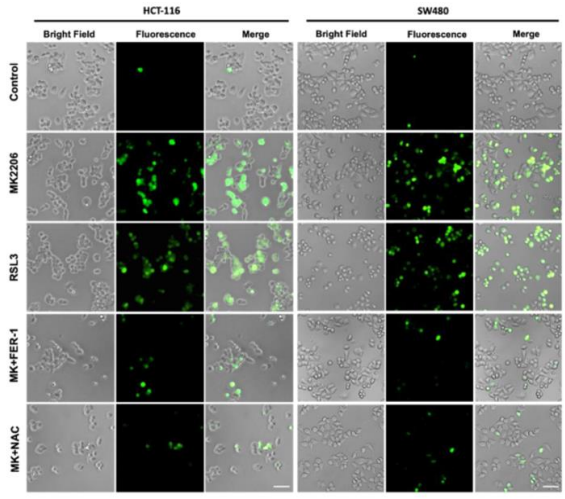

f)

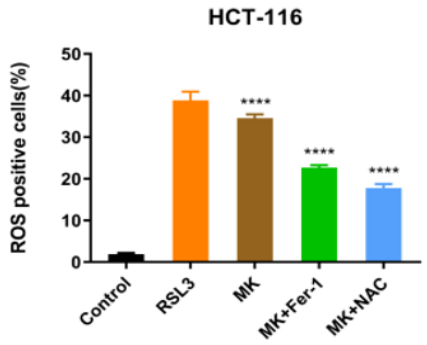

g)

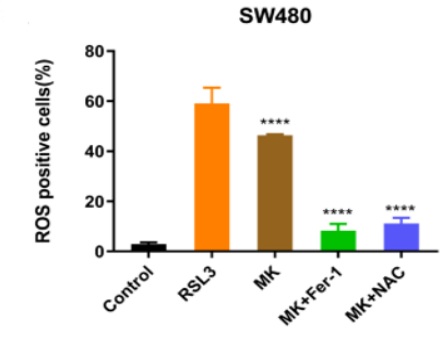

h)

Figure 2. MK2206 induced ferroptosis in CRC cells. a–c) HCT-116 and SW480 cells were treated with 0, 5, and 10 μM MK2206 for 24 h, followed by western blot analysis of GPX4 and β-Actin. d, e) Protein expression of AKT, GPX4, and β-Actin after AKT knockdown. f–h) ROS-positive cells detected by DCFH-DA fluorescence in HCT-116 and SW480 cells treated with MK2206 (10 μM), RSL3 (2 μM), MK2206 + Fer-1 (4 μM), or MK2206 + NAC (20 μM); representative images were captured using a fluorescence microscope [scale bar, 100 μm].

GPX4/ROS-dependent ferroptosis predominantly mediated the inhibition of colon cancer cell proliferation

To further validate the contribution of ferroptosis to growth inhibition, NAC was applied in combination with MK2206. EDU assays showed that the proliferation suppression induced by MK2206 was partially reversed upon NAC co-treatment **(Figure 3a)**, a result corroborated by CCK-8 analysis **(Figures 3g and 3j).** The link between proliferation arrest and ferroptosis was then examined in more detail. As shown in Fig. 3B–E, the reduction in GPX4 expression caused by MK2206 was clearly restored by NAC treatment. Moreover, combined administration of MK2206 and RSL3 exerted a synergistic inhibitory effect on colon cancer cell growth **(Figures 3f and 3i).** In contrast, blocking apoptosis with Z-VAD failed to significantly rescue MK2206-induced growth inhibition **(Figures 3h and 3k),** suggesting that although MK2206 activated both ferroptosis and apoptosis, apoptosis contributed only minimally. Taken together, these results demonstrated that AKT inhibition primarily suppressed colon cancer cell proliferation through GPX4/ROS-dependent ferroptosis.

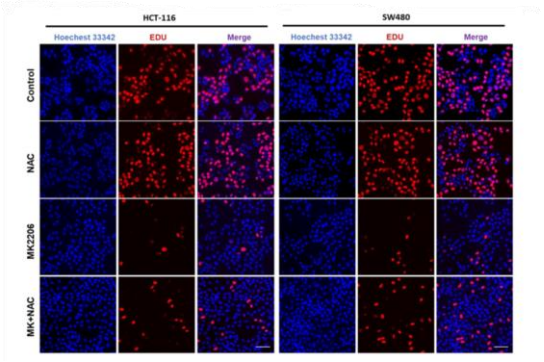

a)

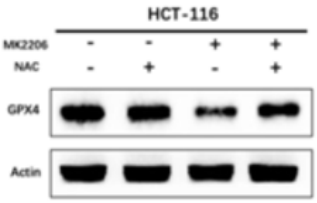

b)

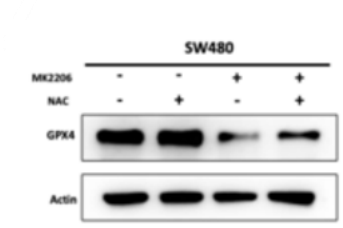

c)

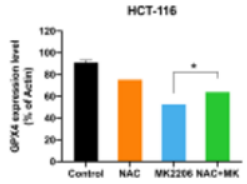

d)

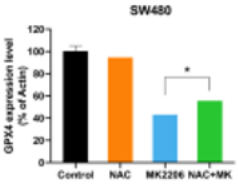

e)

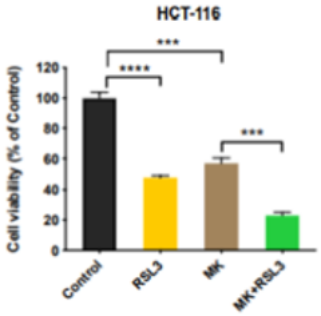

f)

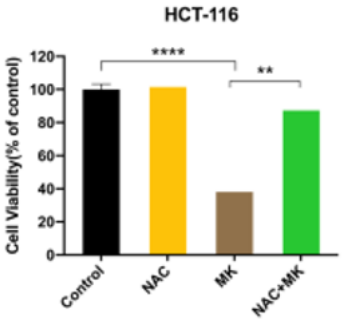

g)

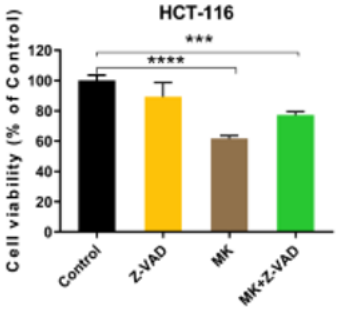

h)

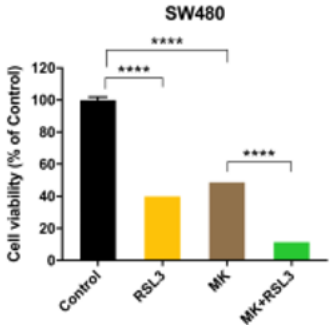

i)

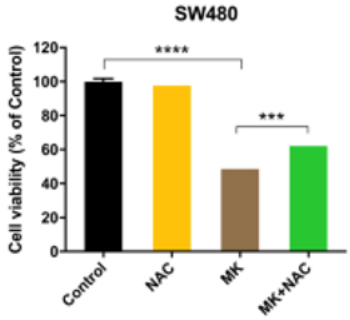

j)

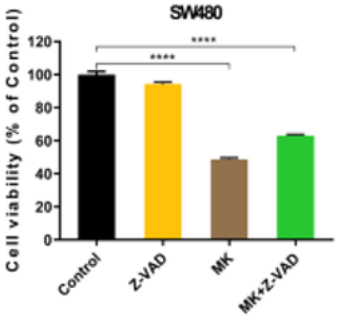

k)

Figure 3. MK2206-induced cell death was attenuated by NAC.

a) EDU assays were performed to evaluate proliferative capacity in HCT-116 and SW480 cells treated with

MK2206, NAC, or MK2206 + NAC [scale bar, 100 μm].

b–e) GPX4 protein levels were analyzed in HCT-116 and SW480 cells following exposure to MK2206, NAC, or MK2206 + NAC.

f–k) Cell proliferation was assessed by CCK-8 assays after combined treatment of MK2206 with RSL3, NAC, or Z-VAD.

AKT inhibition led to FTO downregulation and subsequent reduction of GPX4 expression

We observed that FTO expression was markedly decreased upon AKT suppression **(Figure 4a)**, a finding further validated after AKT knockdown **(Figure 4b)**. To determine whether elevated m6A methylation resulting from FTO loss contributed to ferroptosis regulation, the FTO inhibitor FB23-2 was applied, which significantly reduced GPX4 protein levels as detected by western blotting **(Figure 4c)**. Moreover, CRC cells transfected with FTO siRNA exhibited decreased GPX4 expression, confirming that FTO positively regulates GPX4 expression **(Figure 4d)**. To investigate methylation-related alterations in clinical samples, immunohistochemical staining of tumor tissues revealed higher FTO expression in cancer tissues compared with adjacent non-tumor tissues, whereas METTL3 levels showed no significant difference between the two groups **(Figure 4e)**. In addition, AKT, FTO, and GPX4 were all expressed at higher levels in tumor tissues than in adjacent tissues, suggesting that FTO and GPX4 may serve as potential biomarkers for colorectal cancer. Functionally, inhibition of FTO suppressed cell proliferation; however, this inhibitory effect was largely reversed upon co-treatment with NAC **(Figure 4f)**. Collectively, these findings indicate that m6A methylation plays a critical role in AKT inhibition–induced ferroptosis.

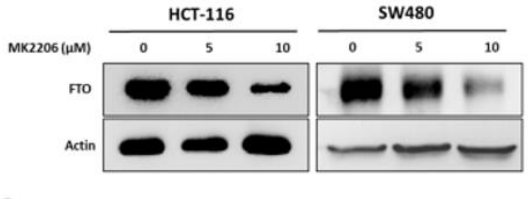

a)

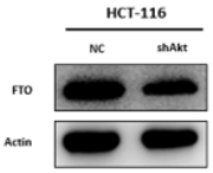

b)

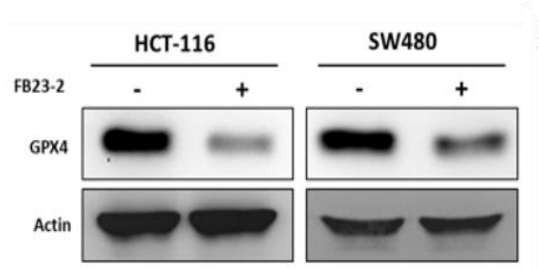

c)

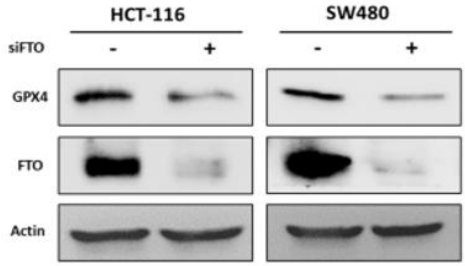

d)

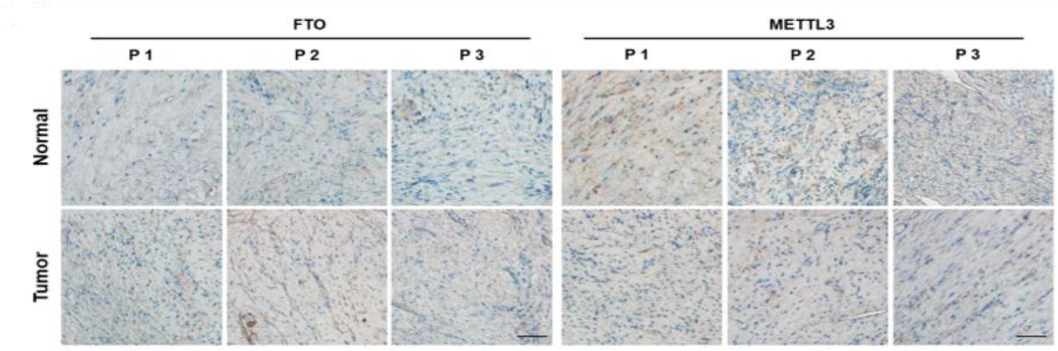

e)

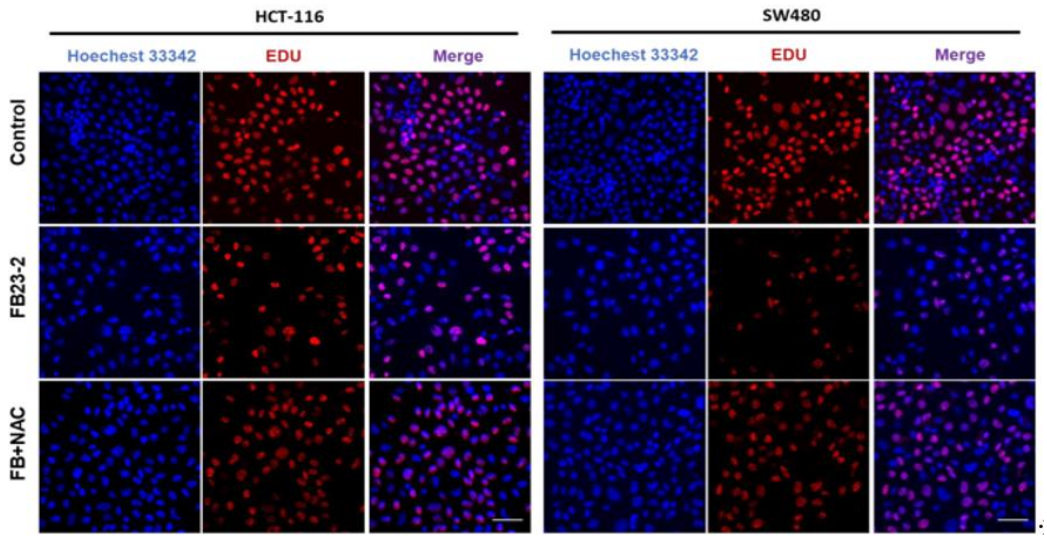

f)

Figure 4. AKT suppression results in reduced FTO expression**.**

a, b) FTO and β-Actin protein levels were examined in HCT-116 and SW480 cells after MK2206 treatment or shAKT transfection.

c) GPX4 and β-Actin expression were analyzed following treatment with the FTO inhibitor FB23-2.

d) Protein levels of GPX4, FTO, and β-Actin were assessed after FTO knockdown.

e) FTO expression was evaluated in clinical colorectal cancer specimens.

f) EDU assays were used to compare proliferation in HCT-116 and SW480 cells treated with FB23-2 alone or FB23-2 + NAC [scale bar, 100 μm].

FTO inhibition elevated GPX4 m6A methylation, which was recognized by YTHDF2 and promoted mRNA degradation

To verify the involvement of m6A modification in AKT inhibition–induced ferroptosis, potential methylation sites at positions 193, 647, and 766 on GPX4 mRNA were predicted using SRAMP, and increased global m6A levels were detected by dot blot analysis **(Figures 5a and 5b).** Site-specific primers were subsequently designed, and Me-RIP assays confirmed that site 193 on GPX4 mRNA represents the authentic m6A modification site **(Figures 5c and 5d)**. To elucidate the regulatory mechanism governing GPX4 m6A modification, YTHDF1, YTHDF2, and YTHDF3 were individually silenced, yielding effective knockdown results **(Figures 5e–5g)**. CCK-8 assays demonstrated that the MK2206-induced reduction in cell proliferation was partially reversed following YTHDF2 interference **(Figures 5h–5j).** As YTHDF2 is known to recognize m6A-modified mRNA and facilitate its degradation [24], its knockdown led to increased GPX4 mRNA abundance **(Figure 5k).** Furthermore, RIP assays revealed enhanced binding between YTHDF2 and GPX4 mRNA upon FTO silencing **(Figures 5l and 5m).** Consistently, western blot analyses showed that MK2206-mediated GPX4 downregulation was alleviated by YTHDF2 inhibition, indicating that YTHDF2 reduces GPX4 protein expression by promoting degradation of its mRNA **(Figures 5n and 5o).** In summary, FTO directly controlled m6A modification of GPX4 mRNA at site 193, while YTHDF2 mediated AKT inhibition–induced ferroptosis by recognizing and degrading m6A-modified GPX4 transcripts.

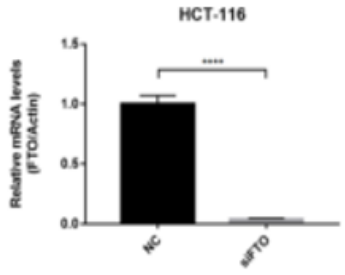

a)

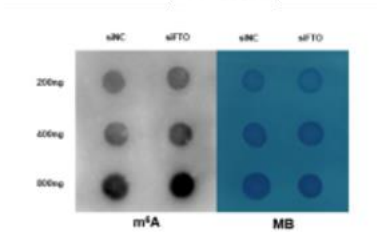
siNC
siFTO
siNC
siFTO
200ng
400ng
800ng
m⁶A
MB

b)

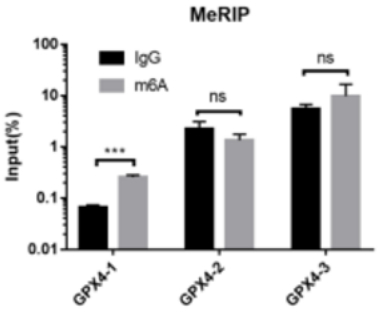
MeRIP
IgG
m6A
Input(%)
100
10
1
0.1
0.01
***
ns
ns
GPX4-1
GPX4-2
GPX4-3

c)

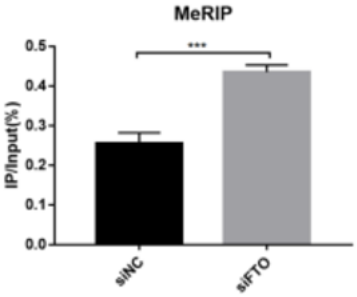
MeRIP
***
IP/Input(%)
0.5
0.4
0.3
0.2
0.1
0.0
siNC
siFTO

d)

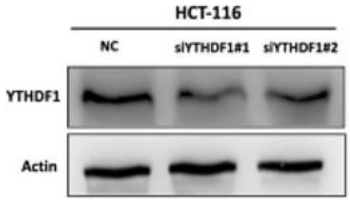
HCT-116
NC
siYTHDF1#1
siYTHDF1#2
YTHDF1
Actin

e)

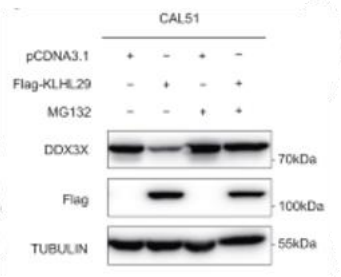
CAL51
pCDNA3.1
Flag-KLHL29
MG132
DDX3X
Flag
TUBULIN
70kDa
100kDa
55kDa

f)

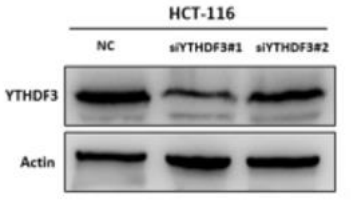
HCT-116
NC
siYTHDF3#1
siYTHDF3#2
YTHDF3
Actin

g)

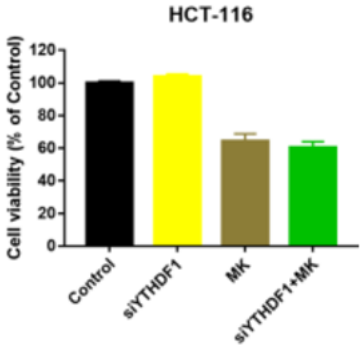
HCT-116
Cell viability (% of Control)
120
100
80
60
40
20
0
Control
siYTHDF1
MK
siYTHDF1+MK

h)

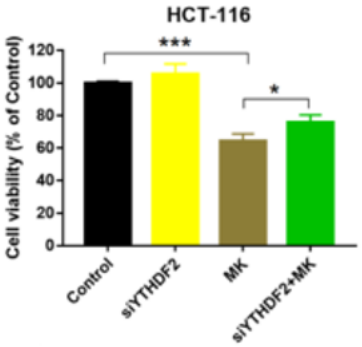
HCT-116
***
*
Cell viability (% of Control)
120
100
80
60
40
20
0
Control
siYTHDF2
MK
siYTHDF2+MK

i)

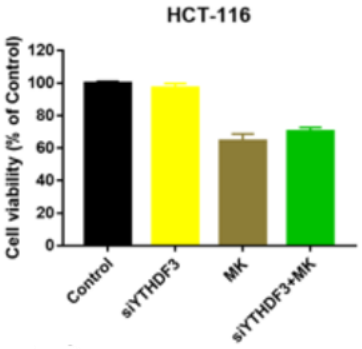
HCT-116
Cell viability (% of Control)
120
100
80
60
40
20
0
Control
siYTHDF3
MK
siYTHDF3+MK

j)

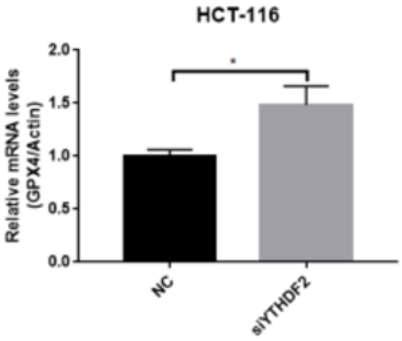

k)

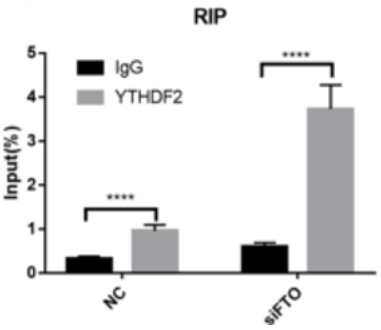

l)

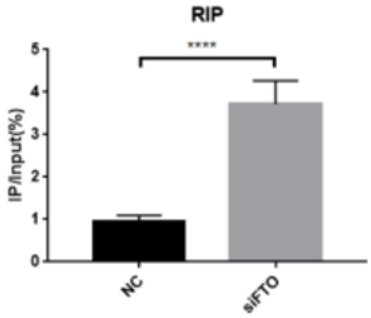

m)

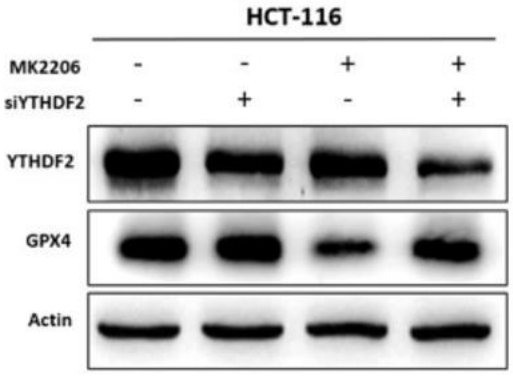

n)

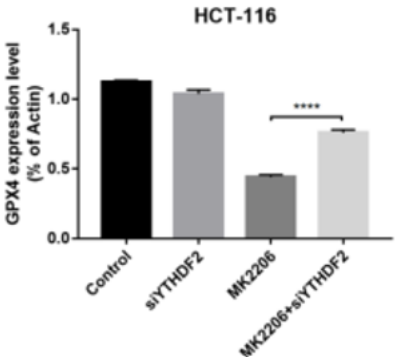

o)

Figure 5. YTHDF2 modulated GPX4 expression**.**
a, b) Dot blot analyses were performed in the NC and siFTO groups.
c, d) MeRIP–qPCR assays were conducted following FTO silencing.
e–g) Knockdown efficiencies of YTHDF1, YTHDF2, and YTHDF3 were validated by western blotting.
h–j) Cell proliferative capacity was evaluated using the CCK-8 assay after YTHDF1, YTHDF2, and YTHDF3 knockdowns.
k–m) RIP assays using YTHDF2 were carried out after FTO knockdown.
n, o) Protein levels of GPX4, YTHDF2, and β-Actin were examined following YTHDF2 silencing and MK2206 treatment.

Autophagy inhibition potentiated MK2206-induced cell death

To determine whether MK2206 simultaneously induced autophagy during ferroptosis activation, CRC cells were exposed to increasing concentrations of MK2206, and LC3 expression was assessed. The LC3-II/LC3-I ratio increased in a dose-dependent manner **(Figures 6a–6c),** indicating autophagy induction. This phenomenon was further confirmed by immunofluorescence analysis after MK2206 treatment. In subsequent experiments, GPX4 expression was markedly lower in cells treated with MK2206 combined with chloroquine (CQ) compared with MK2206 alone **(Figures 6d–5g).** Proliferation of HCT-116 and SW480 cells was examined by EDU assays following treatment with MK2206, MK2206 + CQ, RSL3, and RSL3 + CQ (Fig. S6A, B). Moreover, CCK-8 assays showed that cell proliferation was further suppressed by combined treatment with MK2206 + CQ, RSL3 + CQ, or RSL3 + DC661 **(Figures 6h–6m).** These findings indicate that autophagy serves a protective function against AKT inhibition–induced ferroptosis in

colorectal cancer, and that blocking autophagy enhances MK2206-triggered ferroptotic cell death.

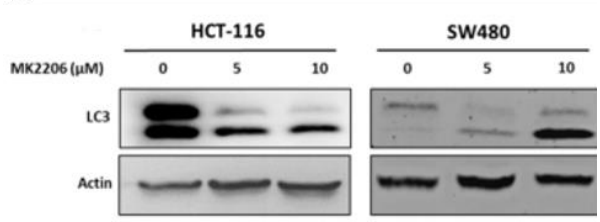

a)

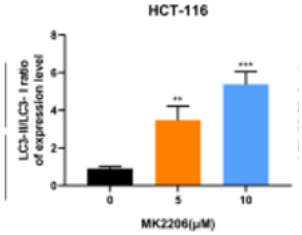

b)

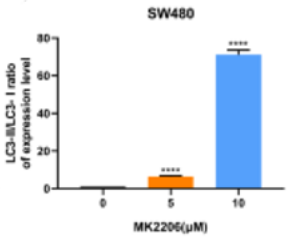

c)

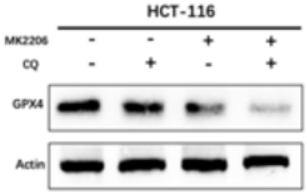

d)

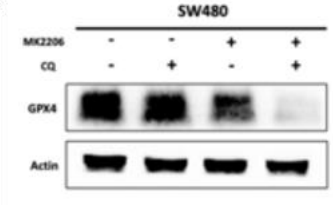

e)

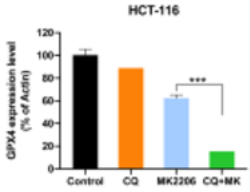

f)

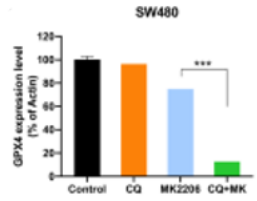

g)

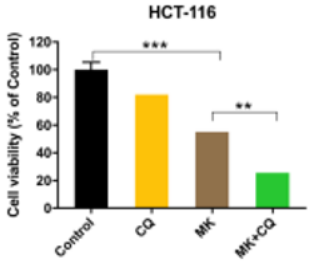

h)

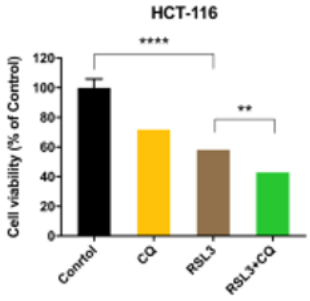

i)

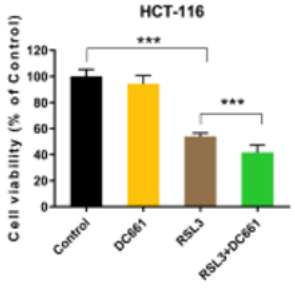

j)

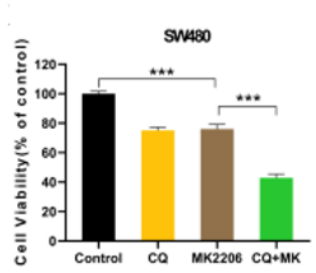

k)

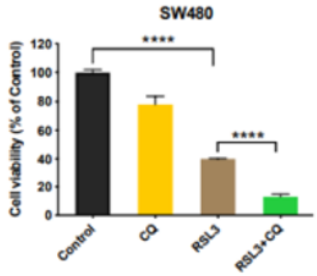

l)

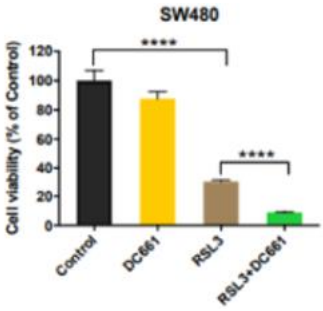

m)

Figure 6. Association between MK2206 treatment and autophagy.

a–c) LC3 and β-Actin protein levels were analyzed following MK2206 exposure.

d–g) GPX4 and β-Actin expression were assessed after treatment with MK2206 and CQ.

h–m) Cell proliferation was measured using the CCK-8 assay after treatment with MK2206, CQ, RSL3, and DC661.

Combined MK2206 and CQ therapy enhanced antitumor efficacy in vivo

To validate these findings in vivo, a CRC xenograft model was established in nude mice to evaluate whether combined administration of MK2206 and CQ produced superior antitumor effects. Tumor volume and weight were reduced in the MK2206-treated group compared with controls, while further reductions were observed in the MK2206 + CQ group relative to MK2206 alone, with no significant changes in body weight among mice **(Figures 7a–7d).** These results demonstrated that combination therapy exerted enhanced antitumor activity. Additionally, immunohistochemical staining of GPX4 and Ki-67 in tumor tissues revealed expression patterns consistent with the in vitro findings **(Figure 7e)**. Collectively, these data indicate that MK2206 suppresses CRC progression by inducing ferroptosis both in vitro and in vivo, and that autophagy inhibition amplifies this effect. Finally, a schematic illustration summarizing the m6A- and autophagy-related ferroptosis regulatory mechanism is presented **(Figure 8).**

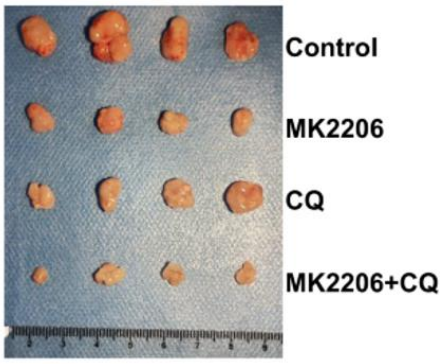

a)

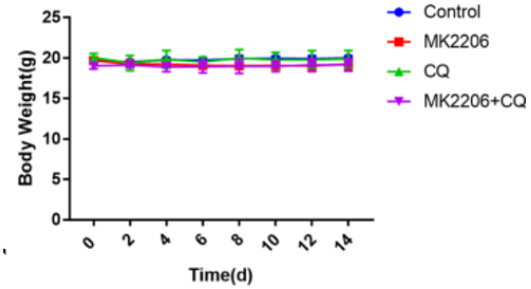

b)

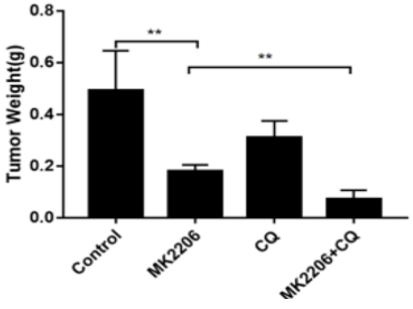

c)

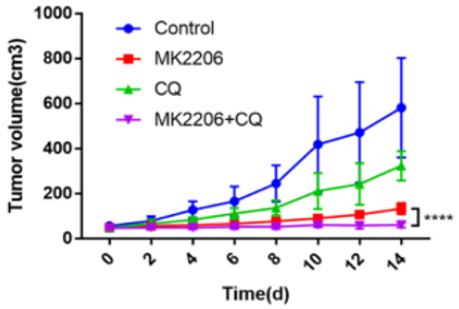

d)

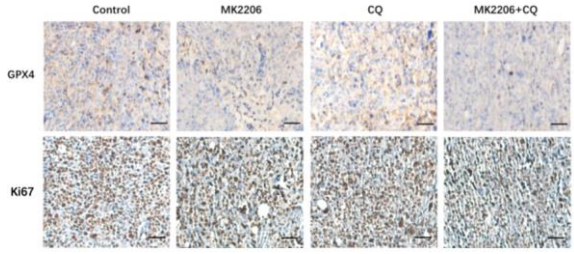

e)

Figure 7. In vivo antitumor effects of MK2206 and CQ. a) Representative image of xenograft tumors. b) Mouse body weights were recorded twice weekly after treatment. C Mean tumor weights were calculated. d) Tumor volumes were measured twice weekly after 0treatment. e Immunohistochemical staining of GPX4 and Ki-67.

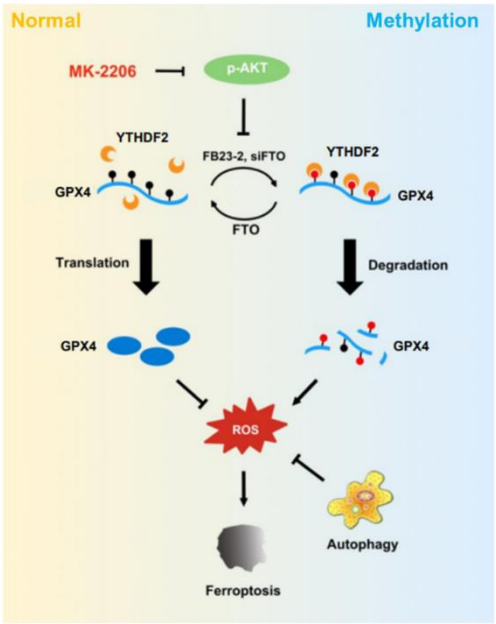

Figure 8. Schematic overview of the study mechanism.

AKT targeting induces ferroptosis through methylation-dependent regulation.

The PI3K–AKT signaling cascade is critically involved in the initiation and progression of numerous malignancies [5]. Aberrant activation of this pathway promotes tumor cell proliferation and growth, with phosphorylated AKT (P-AKT) representing the predominant active form [25]. Previous work by Yi *et al*. demonstrated that the PI3K–AKT–mTOR axis suppresses ferroptosis through SREBP-driven lipogenesis, and that pathway inhibition enhances ferroptosis induction and improves antitumor efficacy [26]. Cai *et al*. reported that blocking AKT–mTOR signaling reduced GPX4 expression in glioblastoma, while Zhang *et al*. showed that mTORC1 partially regulates GPX4 protein synthesis via the mTORC1–4EBP pathway [27, 28]. To clarify the relationship between 4EBP1 and GPX4 following MK2206 exposure, we examined P-4EBP1 and total 4EBP1 together with P-AKT, AKT, and GPX4. In HCT-116 cells, P-4EBP1 levels were markedly reduced after treatment with 1 or 2 μM MK2206, whereas GPX4 expression remained largely unchanged under these conditions. Conversely, GPX4 levels were clearly decreased after exposure to 5 or 10 μM MK2206, without a corresponding reduction in P-4EBP1. In SW480 cells, P-4EBP1 exhibited no obvious decline across 1, 2, 5, or 10 μM MK2206 treatments. Notably, P-AKT and GPX4 displayed similar expression patterns, suggesting that GPX4 functions downstream of AKT rather than 4EBP1. These findings indicate the existence of a regulatory route distinct from previously described pathways in colorectal cancer cells. In this study, inhibition of AKT phosphorylation significantly suppressed tumor growth both in vivo and in vitro, accompanied by reduced FTO and GPX4 expression **(Figures 1 and 7).** Since GPX4 downregulation is closely associated with ferroptosis induction [29] and FTO serves as a key m6A demethylase [30], the concurrent reduction of FTO and GPX4 following AKT inhibition prompted us to investigate the interplay between RNA methylation and ferroptosis in CRC.

Ferroptosis is characterized by iron accumulation and lipid peroxidation and differs fundamentally from other forms of regulated cell death, playing essential roles in diverse biological processes [31]. It is also increasingly recognized as a critical modulator of tumorigenesis. For instance, ELOVL5 and FADS1 were shown to enhance ferroptosis sensitivity and antitumor effects in gastric

cancer [32], while inhibition of SLC7A11 induced ferroptosis in breast cancer [33]. A deeper understanding of ferroptosis in CRC may therefore provide novel therapeutic opportunities. In 2014, Wan *et al*. identified GPX4 as a central regulator of ferroptosis [12], capable of protecting tumor cells from ferroptotic death and thereby influencing therapeutic outcomes [34, 35]. Consequently, elucidating mechanisms governing GPX4 regulation is crucial for ferroptosis-based cancer therapies. Although AKT has been reported to interact with ferroptosis pathways [26, 36], the precise relationship between AKT and GPX4 has remained elusive. In our study, treatment of CRC cells with the AKT inhibitor MK2206 triggered ferroptosis, markedly suppressed GPX4 expression, and increased ROS accumulation. Importantly, expression of FTO, an m6A demethylase, was also reduced during this process, prompting further investigation into the molecular link between methylation dynamics and AKT inhibition–induced ferroptosis.

As the most prevalent internal RNA modification in eukaryotic cells, m6A methylation exerts diverse regulatory effects in both physiological and pathological contexts. In many cancers, m6A modifications are implicated in tumor initiation and progression [36-39]. In CRC, m6A methylation represents a key regulatory layer: Li *et al*. demonstrated that METTL3 promotes CRC progression via IGFBP2 [40], whereas Chen *et al*. reported that METTL14 suppresses tumor growth through the miR-375/YAP1 axis [41]. Increasing evidence has also linked m6A regulation to ferroptosis. Fan *et al*. showed that METTL14 inhibits ferroptosis in hepatocellular carcinoma by activating SLC7A11 through YTHDF2 [42], and YTHDC2 was identified as an endogenous ferroptosis inducer via targeting SLC3A2 in lung adenocarcinoma [43]. Nevertheless, the specific connection between m6A modification and GPX4 regulation has remained unclear. In the present study, we provide initial evidence that m6A methylation modulates ferroptosis by increasing GPX4 m6A levels through FTO inhibition, thereby promoting YTHDF2-mediated GPX4 mRNA degradation. Using SRAMP prediction [44], we identified candidate m6A sites on GPX4 mRNA and experimentally confirmed site 193 as an FTO-regulated methylation locus. During this regulatory process, m6A readers play decisive roles by recognizing modified transcripts and determining their fate [45]. YTHDF2, in particular, is known to bind m6A-modified mRNAs and facilitate their degradation, thereby influencing cell progression [23]. Our findings establish YTHDF2 as the principal m6A reader governing GPX4 methylation and degradation.

Beyond methylation control, multiple additional mechanisms contribute to ferroptosis regulation [46]. Autophagy, for example, has been shown to play a crucial role in ferroptosis modulation [47-48], and nanoparticle-induced ferritinophagy can promote ferroptotic cell death [49]. Autophagy may function as either a protective or destructive process in cancer, depending on context [50]. Our previous studies demonstrated a cytoprotective role of autophagy in CRC [22, 51]. Consistent with these findings, the current study revealed that combined treatment with MK2206 and chloroquine (CQ) significantly reduced GPX4 expression and enhanced ferroptosis. Both cellular and animal experiments confirmed that autophagy inhibition potentiated the antitumor efficacy of MK2206 (Figures 6 and 7), indicating that autophagy exerts a cell death–protective effect following AKT suppression in CRC. These observations highlight autophagy as a potential therapeutic target to overcome resistance and support novel combination strategies for CRC treatment.

Conclusion

In summary, this study uncovers a previously unrecognized regulatory mechanism of ferroptosis in colorectal cancer. AKT inhibition promotes ferroptosis by modulating FTO-dependent demethylation, leading to YTHDF2-mediated GPX4 degradation, with m6A site 193 identified as the critical modification locus. Concurrently, we demonstrate that autophagy functions as a protective mechanism during AKT inhibition–induced ferroptosis. Together, these findings provide new insights that may inform future therapeutic strategies for CRC.

Acknowledgments: We would like to thank all those who have provided financial and technical support for this study. We would like to thank the support of the National Natural Science Foundation of China (82273172), the Clinical Medical Technology Innovation Guidance Project of Hunan Province (2020SK53608), the Project of Henan Health Department (Nos. YXKC2020029/2020054 and SBGJ201901049/2020002041), the Excellent Youth Fund of Henan Natural Science Foundation (No. 212300410075) and the Funding for Scientific Research

and Innovation Team of The First Affiliated Hospital of Zhengzhou University (QNCXTD2023022).

Conflict of Interest: None

Financial Support: None

Ethics Statement: None

References

1. Strickler JH, Yoshino T, Graham RP, Siena S, Bekaii-Saab T. Diagnosis and treatment of ERBB2-positive Metastatic colorectal cancer: a review. JAMA Oncol. 2022. https://doi.org/10.1001/jamaoncol.2021.8196.
2. Sung H, Ferlay J, Siegel RL, Laversanne M, Soerjomataram I, Jemal A, et al. Global cancer statistics 2020: GLOBOCAN estimates of incidence and mortality worldwide for 36 cancers in 185 countries. CA Cancer J Clin. 2021;71:209–49.
3. O'Connell JB, Maggard MA, Ko CY. Colon cancer survival rates with the new American Joint Committee on Cancer sixth edition staging. J Natl Cancer Inst. 2004;96:1420–5.
4. Latres E, Amini AR, Amini AA, Griffiths J, Martin FJ, Wei Y, et al. Insulin-like growth factor-1 (IGF-1) inversely regulates atrophy-induced genes via the phosphatidylinositol 3-kinase/Akt/mammalian target of rapamycin (PI3K/Akt/mTOR) pathway. J Biol Chem. 2005;280:2737–44.
5. Song M, Bode AM, Dong Z, Lee MH. AKT as a therapeutic target for cancer. Cancer Res. 2019;79:1019–31.
6. Zhang Y, Zhang C, Li J, Jiang M, Guo S, Yang G, et al. Inhibition of AKT induces p53/SIRT6/PARP1-dependent parthanatos to suppress tumor growth. Cell Commun Signal CCS. 2022;20:93–110.
7. Dixon SJ, Stockwell BR. The role of iron and reactive oxygen species in cell death. Nat Chem Biol. 2014;10:9–17.
8. Zou Y, Palte MJ, Deik AA, Li H, Eaton JK, Wang W, et al. A GPX4-dependent cancer cell state underlies the clear-cell morphology and confers sensitivity to ferroptosis. Nat Commun. 2019;10:1617.
9. Bedoui S, Herold MJ, Strasser A. Emerging connectivity of programmed cell death pathways and its physiological implications. Nat Rev Mol Cell Biol. 2020;21:678–95.
10. Tsvetkov P, Coy S, Petrova B, Dreishpoon M, Verma A, Abdusamad M, et al. Copper induces cell death by targeting lipoylated TCA cycle proteins. Science. 2022;375:1254–61.
11. Dixon SJ, Lemberg KM, Lamprecht MR, Skouta R, Zaitsev EM, Gleason CE, et al. Ferroptosis: an iron-dependent form of nonapoptotic cell death. Cell. 2012;149:1060–72.
12. Yang WS, SriRamaratnam R, Welsch ME, Shimada K, Skouta R, Viswanathan VS, et al. Regulation of ferroptotic cancer cell death by GPX4. Cell. 2014;156:317–31.
13. Kang R, Tang D. Autophagy and ferroptosis—what's the connection? Curr Pathobiol Rep. 2017;5:153–9.
14. Zhou B, Liu J, Kang R, Klionsky DJ, Kroemer G, Tang D. Ferroptosis is a type of autophagy-dependent cell death. Semin cancer Biol. 2020;66:89–100.
15. Wiener D, Schwartz S. The epitranscriptome beyond m(6)A. Nat Rev Genet. 2021;22:119–31.
16. Deng X, Su R, Weng H, Huang H, Li Z, Chen J. RNA N(6)-methyladenosine modification in cancers: current status and perspectives. Cell Res. 2018;28:507–17.
17. Jiang X, Liu B, Nie Z, Duan L, Xiong Q, Jin Z, et al. The role of m6A modification in the biological functions and diseases. Signal Transduct Target Ther. 2021;6:74–10
18. Oerum S, Meynier V, Catala M, Tisne C. A comprehensive review of m6A/m6Am RNA methyltransferase structures. Nucleic Acids Res. 2021;49:7239–55
19. An Y, Duan H. The role of m6A RNA methylation in cancer metabolism. Mol Cancer. 2022;21:14
20. Zhou J, Wan J, Gao X, Zhang X, Jaffrey SR, Qian SB. Dynamic m(6)A mRNA methylation directs translational control of heat shock response. Nature. 2015;526:591–4.
21. Huang H, Weng H, Sun W, Qin X, Shi H, Wu H, et al. Recognition of RNA N(6)-methyladenosine by IGF2BP proteins enhances mRNA stability and translation. Nat Cell Biol. 2018;20:285–95.
22. Mi W, Wang C, Luo G, Li J, Zhang Y, Jiang M, et al. Targeting ERK induced cell death and p53/ROS-dependent protective autophagy in colorectal cancer. Cell Death Discov. 2021;7:375.

23. Li J, Luo G, Zhang C, Long S, Guo L, Yang G, et al. In situ injectable hydrogel-loaded drugs induce anti-tumor immune responses in melanoma immunochemotherapy. Mater Today Bio. 2022;14:100238
24. Liu J, Duan Z, Guo W, Zeng L, Wu Y, Chen Y, et al. Targeting the BRD4/FOXO3a/CDK6 axis sensitizes AKT inhibition in luminal breast cancer. Nat Commun. 2018;9:5200
25. Wang X, Lu Z, Gomez A, Hon GC, Yue Y, Han D, et al. N6-methyladenosine-dependent regulation of messenger RNA stability. Nature. 2014;505:117–20.
26. Brown JS, Banerji U. Maximising the potential of AKT inhibitors as anti-cancer treatments. Pharm Ther. 2017;172:101–15.
27. Yi JM, Zhu JJ, Wu J, Thompson CB, Jiang XJ. Oncogenic activation of PI3K-AKT-mTOR signaling suppresses ferroptosis via SREBP-mediated lipogenesis. Natl Acad Sci USA. 2020;117:31189–97.
28. Cai JY, Ye Z, Hu YY, Y LG, Gao L, Wang YX, et al. Fatostatin induces ferroptosis through inhibition of the AKT/mTORC1/GPX4 signaling pathway in glioblastoma. Cell Death Dis. 2023. https://doi.org/10.1038/s41419-023-05738-8
29. Zhang Y, Swanda RV, Nie L, Liu X, Wang C, Lee H, et al. mTORC1 couples cyst(e)ine availability with GPX4 protein synthesis and ferroptosis regulation. Nat Commun. 2021;12:1589.
30. Friedmann Angeli JP, Schneider M, Proneth B, Tyurina YY, Tyurin VA, Hammond VJ, et al. Inactivation of the ferroptosis regulator Gpx4 triggers acute renal failure in mice. Nat Cell Biol. 2014;16:1181–912.
31. Jia G, Fu Y, Zhao X, Dai Q, Zheng G, Yang Y, et al. N6-methyladenosine in nuclear RNA is a major substrate of the obesity-associated FTO. Nat Chem Biol. 2011;7:885–7.
32. Shen M, Li Y, Wang Y, Shao J, Zhang F, Yin G, et al. N(6)-methyladenosine modification regulates ferroptosis through autophagy signaling pathway in hepatic stellate cells. Redox Biol. 2021;47:102–151.
33. Lee JY, Nam M, Son HY, Hyun K, Jang SY, Kim JW, et al. Polyunsaturated fatty acid biosynthesis pathway determines ferroptosis sensitivity in gastric cancer. Proc Natl Acad Sci USA. 2020;117:32433–42.
34. Yang J, Zhou Y, Xie S, Wang J, Li Z, Chen L, et al. Metformin induces Ferroptosis by inhibiting UFMylation of SLC7A11 in breast cancer. J Exp Clin Cancer Res. 2021;40:206.
35. Zou Y, Henry WS, Ricq EL, Graham ET, Phadnis VV, Maretich P, et al. Plasticity of ether lipids promotes ferroptosis susceptibility and evasion. Nature. 2020;585:603–8.
36. Viswanathan VS, Ryan MJ, Dhruv HD, Gill S, Eichhoff OM, Seashore-Ludlow B, et al. Dependency of a therapy-resistant state of cancer cells on a lipid peroxidase pathway. Nature. 2017;547:453–7.
37. Wang Q, Chen C, Ding Q, Zhao Y, Wang Z, Chen J, et al. METTL3-mediated m(6)A modification of HDGF mRNA promotes gastric cancer progression and has prognostic significance. Gut. 2020;69:1193–205.
38. Han J, Wang JZ, Yang X, Yu H, Zhou R, Lu HC, et al. METTL3 promote tumor proliferation of bladder cancer by accelerating pri-miR221/222 maturation in m6A-dependent manner. Mol Cancer. 2019;18:110.
39. Cheng M, Sheng L, Gao Q, Xiong Q, Zhang H, Wu M, et al. The m(6)A methyltransferase METTL3 promotes bladder cancer progression via AFF4/NF-kappaB/MYC signaling network. Oncogene. 2019;38:3667–80.
40. Chen Y, Peng C, Chen J, Chen D, Yang B, He B, et al. WTAP facilitates progression of hepatocellular carcinoma via m6A-HuR-dependent epigenetic silencing of ETS1. Mol Cancer. 2019;18:127.
41. Li T, Hu PS, Zuo Z, Lin JF, Li X, Wu QN, et al. METTL3 facilitates tumor progression via an m(6)A-IGF2BP2-dependent mechanism in colorectal carcinoma. Mol Cancer. 2019;18:112.
42. Chen X, Xu M, Xu X, Zeng K, Liu X, Sun L, et al. METTL14 suppresses CRC progression via regulating N6-methyladenosine-dependent primary miR-375 processing. Mol Ther. 2020;28:599–612.
43. Fan Z, Yang G, Zhang W, Liu Q, Liu G, Liu P, et al. Hypoxia blocks ferroptosis of hepatocellular carcinoma via suppression of METTL14 triggered YTHDF2-dependent silencing of SLC7A11. J Cell Mol Med. 2021;25:10197–212.
44. Ma L, Zhang X, Yu K, Xu X, Chen T, Shi Y, et al. Targeting SLC3A2 subunit of system XC(-) is essential for m(6)A reader YTHDC2 to be an endogenous ferroptosis inducer in lung

adenocarcinoma. Free Radic Biol Med. 2021;168:25–43.
45. Zhou Y, Zeng P, Li YH, Zhang Z, Cui Q. SRAMP: prediction of mammalian N6-methyladenosine (m6A) sites based on sequence-derived features. Nuc Acids Res. 2016;44:e91
46. Liu T, Wei Q, Jin J, Luo Q, Liu Y, Yang Y, et al. The m6A reader YTHDF1 promotes ovarian cancer progression via augmenting EIF3C translation. Nuc Acids Res. 2020;48:3816–312.
47. Tang D, Chen X, Kang R, Kroemer G. Ferroptosis: molecular mechanisms and health implications. Cell Res. 2021;31:107–25.
48. Chen X, Li J, Kang R, Klionsky DJ, Tang D. Ferroptosis: machinery and regulation. Autophagy. 2021;17:2054–81.
49. Hou W, Xie Y, Song X, Sun X, Lotze MT, Zeh HJ 3rd, et al. Autophagy promotes ferroptosis by degradation of ferritin. Autophagy. 2016;12:1425–8.
50. Qin X, Zhang J, Wang B, Xu G, Yang X, Zou Z, et al. Ferritinophagy is involved in the zinc oxide nanoparticles-induced ferroptosis of vascular endothelial cells. Autophagy. 2021;17:4266–85.
51. Kimmelman AC, White E. Autophagy and tumor metabolism. Cell Metab. 2017;25:1037–43.